

pubs.acs.org/JPCL Letter

Probing Local Optical Fields via Ultralow Frequency Raman Scattering from a Corrugated Probe

Chih-Feng Wang, Alexander B. C. Mantilla, Andrey Krayev, Yi Gu, and Patrick Z. El-Khoury*



Cite This: J. Phys. Chem. Lett. 2023, 14, 8334-8338



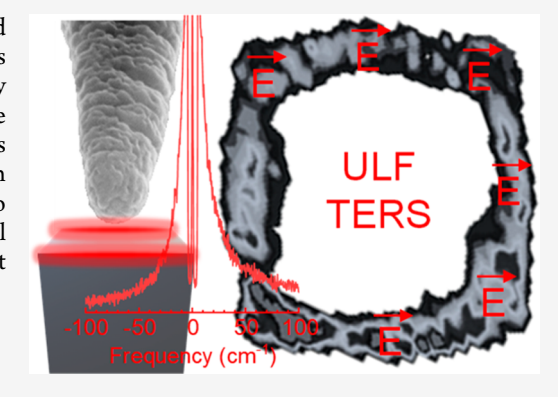
ACCESS I

III Metrics & More

Article Recommendations

s Supporting Information

ABSTRACT: We revisit nanoscale local optical field imaging via tip-enhanced Raman scattering (TERS). Rather than taking advantage of molecular reporters to probe different aspects of the local fields, we show how ultralow frequency Raman (ULF) scattering from the (nanocorrugated) metallic probe itself can be used for the same purpose. The bright ULF-TERS response we record allows non-invasive (tapping mode feedback) local field imaging, enables visualization of the local fields of small (\geq 20 nm) isolated plasmonic particles, and can also be exploited to distinguish between Si and SiO₂ domains with 5 nm spatial resolution. We describe our approach and its limitations, particularly when it comes to using all-metallic versus molecular reporters.



ombining scanning probe microscopy with (non)linear optical spectroscopy achieves the best of both worlds and has led to significant advances in our understanding of molecular and material systems. Several popular techniques have emerged from this combination, including tip-enhanced Raman scattering (TERS²), which allows chemical and chemical reaction imaging with one- to few-nanometer spatial resolution under ambient laboratory conditions. While subnanometer resolution has thus far only been achieved through measurements conducted at ultrahigh vacuum and ultralow temperatures (UHV-ULT), ambient and in situ measurements continue to be important, e.g., in the realms of biological imaging and plasmonic catalysis.

Recent TERS studies have targeted analytes ranging from quantum and semiconductor materials and (bi)metallic catalytic nanostructures to small molecules. Indeed, down to single-molecule detection sensitivity has been observed either directly in UHV-ULT TERS or indirectly under ambient conditions by virtue of the demonstrated spatial resolutions. Beyond chemical imaging, interesting applications of TERS include vibrational mode visualization,4 chemical reaction monitoring,⁶ and direct nano-optical sequencing.⁷ In the same vein, our group has contributed to the field through studies aimed at optical field imaging.³ From visualizing the spatial distributions and vector components of local optical fields to measurements that are sensitive to local optical field resonances, hyperspectral TERS maps indeed contain a wealth of information about the (non)local fields that are acting on nearby molecular and material systems.³

In a recent report from our group, we extended TERS to the ultralow frequency (ULF) domain.⁸ Namely, using smooth

plasmonic probes, we tracked low frequency interlayer phonons in TMD heterostructures. In this work, we combine ULF-TERS with the concept of local optical field imaging via nano-Raman. Rather than relying on molecular reporters, we now use ULF-Raman scattering from a (sputtered) plasmonic probe. The tip-only signal is further enhanced in the vicinity of nanostructures and material systems that further enhance the ULF-Raman signal of the probe. These include isolated plasmonic nanoparticles that are ≥20 nm in diameter. Noninvasive ULF-TERS is possible using tapping mode AFM feedback, by virtue of the large low frequency Raman response compared to conventional Raman scattering from molecules in the fingerprint region. As a direct application of our approach, we show that ULF-TERS from the plasmonic probe can be used to distinguish between Si and SiO2 on the nanoscale, with high sensitivity and a spatial resolution of ~5 nm under ambient conditions.

Because ULF Raman signals are very close to the laser line, caution needs to be exercised to ensure that the recorded low frequency response is indeed inelastic as opposed to a result of laser light leaking through the filters. This is the starting point for our discussion. Beyond engineering controls, i.e., the use of ultranarrow lasers and appropriate ULF notch filters, we performed several initial checks, which are summarized in

Received: July 30, 2023
Accepted: September 7, 2023
Published: September 12, 2023





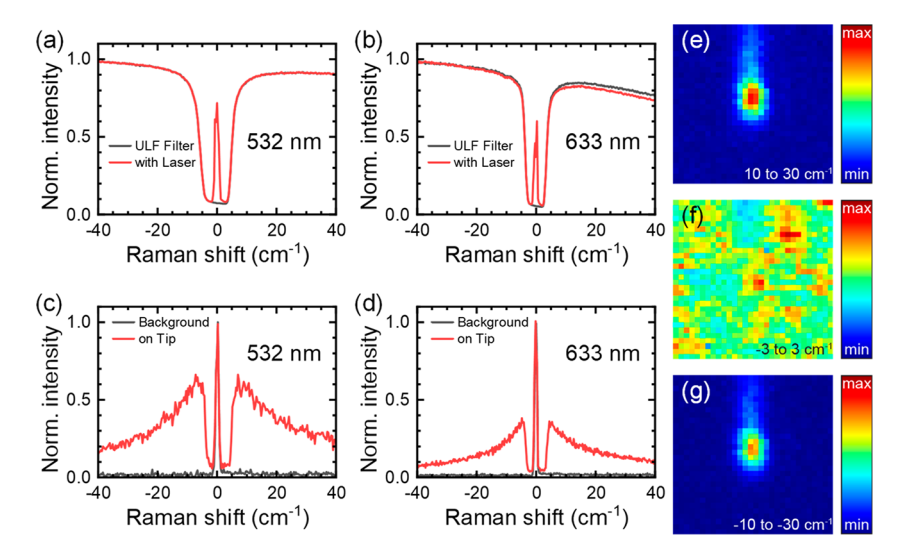


Figure 1. White light transmission through the (a) 532 and (b) 633 nm notch filters with and without laser light. The full widths at half-maxima of the blocking bands are ± 6 and ± 4 cm⁻¹ in panels a and b, respectively. (c and d) Normalized terahertz Raman spectra of a silver-coated AFM tip (Nanosensors, ATEC-NC) at 532 and 633 nm, respectively. These images were taken from hyperspectral micrographs of the probe recorded by using an xyz piezo objective scanner. (e–g) Maps taken from micro-Raman spectral images of a silver-coated AFM tip. The images were integrated in the 10-30 cm⁻¹ range (e), around the laser line in the -3 to 3 cm⁻¹ region (f), and in the -10 to -30 cm⁻¹ spectral region (g). Note that the images were recorded using a 633 nm continuous wave laser and that the entire field of view is 3 μ m in both the vertical and horizontal directions (100 nm step size in both directions). Conditions for the 532 nm measurement: 150 nm AFM tip, 0.5 mW laser power, 0.5 s/pixel integration. Conditions for the 633 nm measurement: 130 nm AFM tip, 0.26 mW laser power, 1 s/pixel integration.

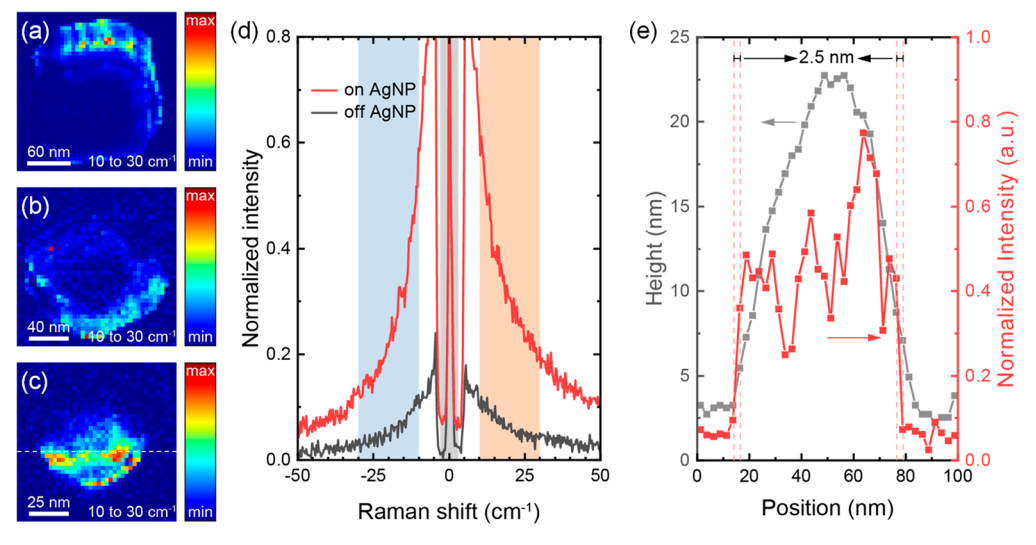


Figure 2. Tapping mode for ULF-TERS imaging of silver nanoparticles on silicon. The ULF-TERS maps depict the results of various silver nanoparticles imaged using a metal-coated AFM tip (Nanosensors, ATEC-NC) in tapping mode. (a and b) ULF-TERS images of 100 nm (nanoComposix, SCPH100) and 55 nm (nanoComposix, SCPH55) silver nanocubes, respectively, using a 633 nm continuous wave laser. (c) A 20 nm silver nanoparticle (Sigma-Aldrich, 730793) irradiated at 532 nm. (d) ULF-TERS spectra normalized to the laser intensity, averaged when the AFM tip is placed on or off the silver nanoparticle in panel c. (e) Line profile of the ULF-TERS response in the Stokes region along the dashed line in panel c.

Figure 1. Panels a and b of Figure 1 show spectra resulting from the transmission of white light through the 532 and 633 notch filters, both with and without laser illumination. Illumination was achieved using a removable in-line camera that can be placed before the objective (side illumination channel) and that is equipped with a built-in white light-emitting diode source. These two plots otherwise show the filter functions and also reveal that the ultranarrow lasers we use are fully contained within the ultrasharp spectral window of null transmission. Panels c and d of Figure 1 show Raman scattering spectra taken on or off plasmonic probes, and they

are obtained by integrating the spectral response contained in a circular area centered around the tip apex or in the blue areas seen in Figure 1e-g. The images (Figure 1e-g) are otherwise obtained by mapping the optical response in space using a xyz piezo objective scanner to which the side illumination objective is mounted. Similar images are typically used to locate the apex of the plasmonic probe prior to nano-optical mapping. From these images, it is immediately evident that the inelastically scattered radiation (both Stokes and anti-Stokes) is nascent from and localized to the apex of the probe. This localization is a prerequisite to the measurements described

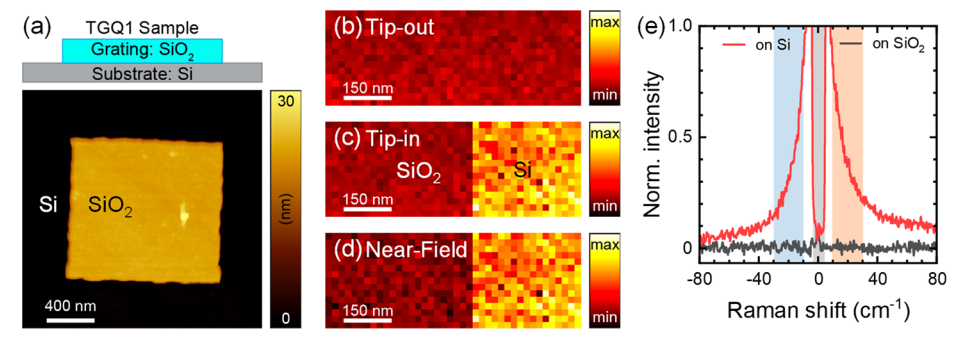


Figure 3. ULF-TERS imaging of dielectric materials. (a) Schematic of the sample, which consists of an AFM calibration standard (NT-MDT, TGQ1). The lower part of the same panel shows a representative topographic AFM map of the substrate. The ULF-TERS images in panels b—d track a small area at the Si–SiO₂ interface. (b and c) ULF-TERS images (averaged between 10 and 30 cm⁻¹) when the tip was retracted and in contact with the substrate, respectively. (d) Pure near-field ULF-TERS image obtained by normalizing the tip-in image using the tip-out response recorded at every pixel. (e) Averaged near-field terahertz Raman spectra on the Si and SiO₂ regions. For this experiment, we utilized a silver-coated AFM tip with a thickness of 100 nm irradiated using a 532 nm continuous wave laser (1.0 mW power). Spectra were otherwise time-integrated for 0.1 s at every pixel.

below. The zero line image (Figure 1f), however, shows no contrast, as it tracks only a small amount of stray laser light as opposed to an optical response. Finally, it is important to note that not all tips we tested were suitable for the measurements described below. ULF Raman signal localization to the apex that results in images similar to those shown in panels e and g of Figure 1 is necessary for high resolution ULF-TERS mapping.

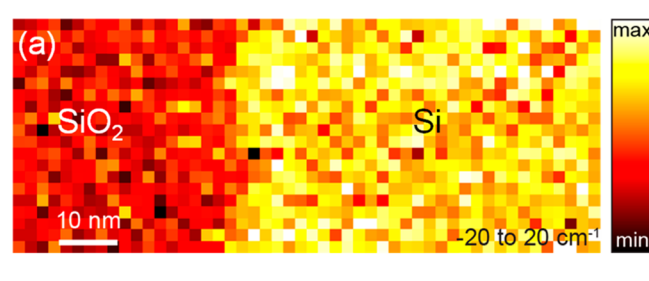
Hyperspectral ULF-TERS images of 100 and 55 nm silver nanocubes are shown in panels a and b, respectively, of Figure 2. Using 633 nm laser excitation, a clear enhancement of the ULF Raman response can be seen. These images are reminiscent of conventional (fingerprint region) TERS images of chemically functionalized plasmonic nanocubes.9 The images trace the edges of the cubes where the local fields defined by the interaction between the plasmonic probe and the edges of the cubes are maximally enhanced. Deviations from square-shaped scattering in this case can be traced back to the heterogeneous morphology of the sputtered metallic probe. 10 Note that these measurements, and unlike most of our prior demonstrations, are performed using tapping mode AFM feedback by virtue of the brightness of the ULF-TERS signal. This allows us to push the limits of our approach to local optical field mapping to smaller plasmonic nanoparticles as tipinduced displacement of the particles is minimal here versus using intermittent AFM feedback. Indeed, the spectral response in intermittent AFM feedback is recorded when the tip is in direct contact with the surface with a preset force value that falls in the repulsive regime, even though pixel-to-pixel motion is still executed using tapping mode AFM. Empirically, this easily causes displacement of silver and gold nanoparticles. Figure 2c shows the TERS map of an irregular 20 nm plasmonic silver nanoparticle. The image was recorded by using a 532 nm laser source to better match the energy of the incident radiation with the resonance of the smaller silver nanoparticle. The visualized local optical field profile is irregular, and it tracks the non-uniform morphology of the particle, as described well elsewhere.

Even though the origin of the contrast that we observe in the images is clear, distinct phenomena can lead to ULF Raman scattering from the probe away from and/or in contact with the nanoparticles (see Figure 2d). The Stokes/anti-Stokes asymmetry observed here can, on one hand, be associated with electronic Raman scattering, as discussed in a recent report.¹¹

That said, enhanced vibrational Raman scattering from heterogeneous metallic nanostructures sustained near the apex of the sputtered plasmonic probe cannot be excluded. Indeed, seminal works in the area of plasmon-enhanced Raman scattering assigned similar observations to localized acoustic vibrations from nanostructures sustained on rough metal films. In practice, it is likely that both phenomena contribute to the recorded signals, and distinguishing between them is difficult in our case of a sputtered plasmonic probe. Nevertheless, our observation of ultrahigh spatial resolution in ULF-TERS (Figure 2e) necessitates that the signal be nascent from small metallic nanostructures on the probe and that the signal be further enhanced at plasmonic junctions defined by the plasmonic probe and plasmonic nanoparticles.

The measurements described above establish that ULF-TERS spectral images report on the spatial profiles of confined and enhanced local optical fields near metallic nanostructures. Our next demonstration takes advantage of a similar effect, namely, enhanced ULF-Raman from the probe, but now on Si versus SiO₂. The substrate can be visualized by using the schematic and topographic AFM map in Figure 3a. It consists of ~20 nm high SiO₂ domains on top of a silicon substrate. Optical imaging of the SiO2 edge in Figure 3a results in the simultaneously recorded tip-out [retracted by ~25 nm from the surface (Figure 3b)] and tip-in spectra [tip in contact with the substrate (Figure 3c)]. Subtracting the former from the latter results in the pure near-field image shown in Figure 3d. Near-field spectra taken when the tip is on Si versus SiO₂ are shown in the same plot in Figure 3e. Our observation of enhanced ULF-TERS on Si versus negligible ULF-TERS on the SiO₂ domain can be understood on the basis of prior analyses. 13 Finite-difference time-domain simulations (not shown) that account for our experimental construct also reveal strongly enhanced local optical fields on Si versus SiO₂. The difference in local optical field enhancement is what generates the observed contrast. Using a lateral step size as small as 2 nm, we establish that the spatial resolution in these measurements is on the order of 6 nm (see Figure 4). This is contrasted with the result shown in Figure 2, where strong interactions between the plasmonic tip and plasmonic nanostructures yield ultraconfined local fields that we track with sub-3 nm spatial resolution.

In conclusion, this work shows that ULF-TERS scattering from a corrugated metallic probe can be used to track local



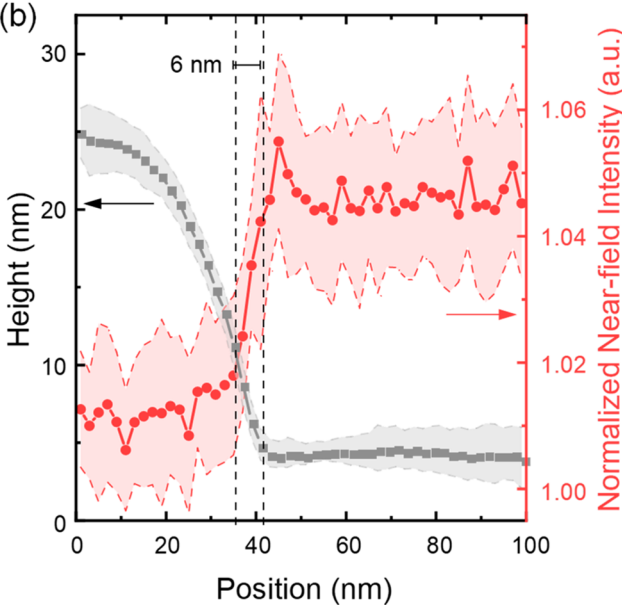


Figure 4. High spatial resolution ULF-TERS image. The results shown here are similar to their analogues in Figure 3, but now using a lateral step size of 2 nm. (a) Image of (integrated in the -20 to $20~{\rm cm}^{-1}$ spectral region) and (b) topographic and ULF-TERS cross-sectional line cuts that traverse the Si–SiO $_2$ interface. Conditions: 532 nm continuous wave laser irradiation (1.3 mW power) with a time integration of 0.2 s/pixel. The pink and gray dashed lines in panel b represent the upper and lower error bars for the normalized near-field intensity and height.

optical fields in the vicinity of metallic and dielectric substrates. Compared to related measurements that rely on molecular reporters, the brightness of the signals from the probe allows tapping mode TERS mapping with a high signal-to-noise ratio. The non-invasive nature of tapping mode TERS allows us to interrogate smaller plasmonic particles, which is currently not trivial using intermittent contact AFM feedback, wherein particles are displaced and even picked up by the probe. The downside of the currently used approach has to do with the limited information content here versus in the case of molecular TERS, where vector components, resonances, and even nature (local vs nonlocal) of local optical fields can be tracked. The current approach, nonetheless, allows us to distinguish between Si and SiO₂ with high sensitivity as a result of dimmer ULF-TERS atop SiO2 versus Si. Given the importance of these structural motifs in emerging (micro)electronics and the semiconductor industry more generally, the approach we describe here could be attractive for emerging research directions.

ASSOCIATED CONTENT

Solution Supporting Information

The Supporting Information is available free of charge at https://pubs.acs.org/doi/10.1021/acs.jpclett.3c02122.

Transparent Peer Review report available (PDF)

AUTHOR INFORMATION

Corresponding Author

Patrick Z. El-Khoury — Physical Sciences Division, Pacific Northwest National Laboratory, Richland, Washington 99352, United States; Orcid.org/0000-0002-6032-9006; Email: patrick.elkhoury@pnnl.gov

Authors

Chih-Feng Wang — Physical Sciences Division, Pacific Northwest National Laboratory, Richland, Washington 99352, United States; © orcid.org/0000-0002-3085-6614

Alexander B. C. Mantilla – Department of Physics and Astronomy, Washington State University, Pullman, Washington 99164, United States; orcid.org/0000-0002-9262-1351

Andrey Krayev — Horiba Instruments, Inc., Novato, California 94949, United States; orcid.org/0000-0001-7590-4002

Yi Gu – Department of Physics and Astronomy, Washington State University, Pullman, Washington 99164, United States

Complete contact information is available at: https://pubs.acs.org/10.1021/acs.jpclett.3c02122

Notes

The authors declare the following competing financial interest(s): Y.G. has equity interest in Klar Scientific.

ACKNOWLEDGMENTS

C.-F.W. was supported by the U.S. Department of Energy, Office of Science, Office of Biological and Environmental Research, through the bioimaging technology development program. A.B.C.M. and Y.G. acknowledge support from the National Science Foundation (DMR-2004655). P.Z.E.-K. acknowledges support from the U.S. Department of Energy, Office of Science, Basic Energy Sciences, Chemical Sciences, Geosciences, and Biosciences Division, Condensed Phase and Interfacial Molecular Science program (FWP 16248).

REFERENCES

- (1) Schultz, J. F.; Mahapatra, S.; Li, L.; Jiang, N. The Expanding Frontiers of Tip-Enhanced Raman Spectroscopy. *Appl. Spectrosc.* **2020**, 74, 1313–1340.
- (2) Stöckle, R. M.; Suh, Y. D.; Deckert, V.; Zenobi, R. Nanoscale Chemical Analysis by Tip-Enhanced Raman Spectroscopy. *Chem. Phys. Lett.* **2000**, *318*, 131–136.
- (3) El-Khoury, P. Z. Tip-Enhanced Raman Scattering on Both Sides of the Schrödinger Equation. *Acc. Chem. Res.* **2021**, *54*, 4576–4583.
- (4) Lee, J.; Crampton, K. T.; Tallarida, N.; Apkarian, V. A. Visualizing Vibrational Normal Modes of a Single Molecule with Atomically Confined Light. *Nature* **2019**, *568*, 78–82.
- (5) Mahapatra, S.; Ning, Y.; Schultz, J. F.; Li, L.; Zhang, J.-L.; Jiang, N. Angstrom Scale Chemical Analysis of Metal Supported Trans- and Cis-Regioisomers by Ultrahigh Vacuum Tip-Enhanced Raman Mapping. *Nano Lett.* **2019**, *19*, 3267–3272.
- (6) Li, Z.; Kurouski, D. Plasmon-Driven Chemistry on Mono- and Bimetallic Nanostructures. *Acc. Chem. Res.* **2021**, *54*, 2477–2487.
- (7) He, Z.; Han, Z.; Kizer, M.; Linhardt, R. J.; Wang, X.; Sinyukov, A. M.; Wang, J.; Deckert, V.; Sokolov, A. V.; Hu, J.; Scully, M. O. Tip-

- Enhanced Raman Imaging of Single-Stranded DNA with Single Base Resolution. J. Am. Chem. Soc. 2019, 141, 753–757.
- (8) Rodriguez, A.; Krayev, A.; Velický, M.; Frank, O.; El-Khoury, P. Z. Nano-Optical Visualization of Interlayer Interactions in WSe₂/WS₂ Heterostructures. *J. Phys. Chem. Lett.* **2022**, *13*, 5854–5859.
- (9) Bhattarai, A.; Novikova, I. V.; El-Khoury, P. Z. Tip-Enhanced Raman Nanographs of Plasmonic Silver Nanoparticles. *J. Phys. Chem.* C **2019**, *123*, 27765–27769.
- (10) Wang, C.-F.; O'Callahan, B. T.; Arey, B. W.; Kurouski, D.; El-Khoury, P. Z. High-Resolution Raman Nano-Imaging with an Imperfect Probe. *J. Phys. Chem. C* **2022**, *126*, 4089–4094.
- (11) Sun, S.; Rathnayake, D. T. N.; Guo, Y. Asymmetrical Spectral Continuum between Anti-Stokes and Stokes Scattering Revealed in Low-Frequency Surface-Enhanced Raman Spectroscopy. *J. Phys. Chem. C* **2022**, *126*, 11193–11200.
- (12) Weitz, D. A.; Gramila, T. J.; Genack, A. Z.; Gersten, J. I. Anomalous Low-Frequency Raman Scattering from Rough Metal Surfaces and the Origin of Surface-Enhanced Raman Scattering. *Phys. Rev. Lett.* **1980**, *45*, 355–358.
- (13) Oldenburg, K.; Hartmann, H.; Lermé, J.; Pohl, M.-M.; Meiwes-Broer, K.-H.; Barke, I.; Speller, S. Virtual Plasmonic Dimers for Ultrasensitive Inspection of Cluster-Surface Coupling. *J. Phys. Chem.* C **2019**, *123*, 1379–1388.